NUMERICAL SIMULATION OF EXTERNAL COMPRESSIBLE FLOWS USING THE IMMERSED BOUNDARY METHOD WITH VIRTUAL PHYSICAL MODEL

Reis M. G. A.*, Lima e Silva A. L. F and Lima e Silva S. M. M.
*Author for correspondence
Institute of Mechanical Engineering,
Federal University of Itajubá,
Itajubá- MG, Brazil,
E-mail: mauricioreis@unifei.edu.br

ABSTRACT

The objective of this study was to apply the Immersed Boundary Method with the Virtual Physical Model to study external compressible flows. The Immersed Boundary methods have been increasingly used to model flows with submerged objects, particularly when they are in movement or deformation. These methods use independent grids to represent the domain and the immersed bodies. The domain is represented by an Eulerian mesh, whereas the 2D immersed body is represented by a set of points, which is called Lagrangian mesh. The no-slip condition is enforced by the force field introduced into the momentum equation. Another advantage of this approach is that the drag and lift forces can be calculated directly by using the Lagrangian force field. In the Virtual Physical Model, the force is first obtained in the Lagrangian grid by using the conservation laws and then is distributed to the Eulerian grid. In the present work, a non-uniform Cartesian grid and a central finite volume scheme with second order accuracy were used in the spatial discretization of the Navier-Stokes equations. The Euler method was applied for time discretization. Subsonic flows were simulated over a circular profile with adiabatic walls for different Reynolds numbers. Supersonic shock wave reflection problems were also simulated. Relevant parameters such as drag and lift forces, Strouhal number and pressure distribution were compared with numerical and experimental results from literature. In addition, this study was carried out using OpenFOAM program, seeking to validate the methodology and the in-house CFD code developed in this work.

INTRODUCTION

Many researchers have been interested in studying flows over immersed bodies due to their different applicabilities. The Immersed Boundary Method (IBM), proposed by Peskin [1], was first developed to be applied in the modeling of elastic boundaries immersed in incompressible viscous flows. In this methodology, the conservative equations are solved by using an Eulerian grid that represent the whole domain, and a Lagrangian grid is used to represent the immersed body. The effect of the immersed body is felt through a force field $\mathbf{f}$ added to the momentum equations acting on the interface region and its neighborhoods. Later, different IBM approaches have been suggested in literature, such as cut-cell method [2] and the ghost-cell method [3]. The cut-cell approach involves truncating the Cartesian cells at the boundary surface to create new cells which conform to the shape of the surface. In ghost-cell approach, a ghost zone is introduced near the boundaries and within the solid body.

At the present work, the Immersed Boundary Method (IBM) and the Physical Virtual Model (VPM) [4] were used to study external compressible flows in subsonic and supersonic regime.

NOMENCLATURE

c	[m/s]	Speed of sound
CFL	[-]	Courant number
C_d	[-]	Drag coefficient
C_l	[-]	Lift coefficient
c_p	[J/kgK]	Heat capacity at constant pressure
D	[m]	Diameter of the cylinder
D_{ij}	$[m^{-2}]$	Distribution/interpolation function
e	[J/kg]	specific total energy
$\mathbf{f}$	$[N/m^3]$	Eulerian Force vector
$\mathbf{F}$	$[N/m^3]$	Lagrangian Force vector
I	[-]	Indicator function
k	[W/mK]	Thermal conductivity
Ma	[-]	Mach number
MM	[g/mol]	Molar mass
N_P	[-]	Number of Lagrangian points
p	[Pa]	Pressure
Pr	[-]	Prandtl number
q_x	$[W/m^2]$	Heat flux by conduction in x direction
q_y	$[W/m^2]$	Heat flux by conduction in y direction
Re	[-]	Reynolds number
St	[-]	Strouhal number
t	[s]	time
T	[K]	Temperature
$\mathbf{U}$	[m/s]	Vector velocity in Cartesian mesh
u, v	[m/s]	Velocity components in the x and y directions
$\mathbf{x}$	[m]	Vector position in Cartesian mesh
x, y	[m]	Cartesian axis directions

Special characters

ρ	$[kg/m^3]$	Density
γ	[-]	Heat capacity ratio
κ	[W/mK]	Thermal conductivity
ψ	[-]	Non-dimensional time
μ	[Pa s]	Dynamic viscosity
θ	[-]	angle
τ	$[N/m^2]$	Viscous stress tensor
$\Delta x, \Delta y$	[m]	Cell dimensions in x and y directions
Δs	[m]	Distance between Lagrangian points

Subscripts

∞	Undisturbed flow
min	Minimum value

The VPM, which is a model to calculate the Lagrangian force **F** on the immersed body, was initially developed for incompressible flows, and in the present work was extended to compressible flows.

A numerical C++ code named Compressible Virtual Physical Model (CVPM) was developed to solve the compressible Navier-Stokes equations (NSE) in a Cartesian grid. This in-house code is based on the IBM/VPM to model the immersed objects. The studied cases were also simulated using the OpenFOAM program (OF) which uses adaptive grids to solve external flows making it a good alternative to validate comparing the results. Literature data were also used in validations.

MATHEMATICAL MODEL

The compressible, two-dimensional Navier-Stokes equations, mass, momentum and energy can be written in Cartesian coordinates as:

$$\frac{\partial \mathbf{Q}}{\partial t} = -\frac{\partial \mathbf{F}}{\partial x} - \frac{\partial \mathbf{G}}{\partial y} + \frac{\partial \mathbf{F}_v}{\partial x} + \frac{\partial \mathbf{G}_v}{\partial y} + \mathbf{f} \tag{1}$$

where:

$$\mathbf{Q} = \left| \rho \quad \rho u \quad \rho v \quad \rho e \right|^T \tag{2}$$

$$\mathbf{F} = \left| \rho u \quad \rho u^2 + p \quad \rho uv \quad u(\rho e + p) \right|^T \tag{3}$$

$$\mathbf{G} = \left| \rho v \quad \rho uv \quad \rho v^2 + p \quad v(\rho e + p) \right|^T \tag{4}$$

$$\mathbf{F}_v = \left| 0 \quad \tau_{xx} \quad \tau_{xy} \quad u\tau_{xx} + v\tau_{xy} - q_x \right|^T \tag{5}$$

$$\mathbf{G}_v = \left| 0 \quad \tau_{yx} \quad \tau_{yy} \quad u\tau_{yx} + v\tau_{yy} - q_y \right|^T \tag{6}$$

$$\mathbf{f} = \left| 0 \quad f_x \quad f_y \quad 0 \right|^T \tag{7}$$

In vector **Q**, there are conservative quantities in its intensive forms: mass, momentum and energy; thus the term on the left of equation (1) represents its rates of change with time. Vectors **F** and **G** are terms of advective transport of these variables, and $\mathbf{F}_v$ and $\mathbf{G}_v$ are terms of diffusive transport. τ_{ij} are the components of the viscous stress tensor. By considering the fluid as Newtonian and non-polar, and the Stokes hypotheses the terms of the viscous stress tensor can be calculated as:

$$\tau_{ij} = \mu \left(\frac{\partial \mathbf{U}_j}{\partial x_i} + \frac{\partial \mathbf{U}_i}{\partial x_j} \right) - \frac{2}{3}\mu \frac{\partial \mathbf{U}_i}{\partial x_i} \delta_{ij} \tag{8}$$

In equations (5) and (6), q_x and q_y are the conduction heat flux in each coordinate that conforms to Fourier's law.

The system of equations becomes complete by using a state law for the fluid considered as an ideal gas:

$$p = \rho(\gamma - 1)\left(e - \frac{u^2 + v^2}{2} \right), \tag{9}$$

Mathematical modeling of the Immersed Boundary

Two meshes are used in IBM named Eulerian and lagrangian meshes. In the Eulerian mesh, the discretized governing equations are solved and the Lagrangian mesh is used to represent the immersed boundaries. The Lagrangian grid for a two-dimensional flow is formed by a set of points called Lagrangian points. These points are represented by the subscript $_k$, so its position is vector $\mathbf{x}_k$.

In the VPM approach, the force field $\mathbf{F}(\mathbf{x}_k, t)$ which complies with the conditions of non-slip and non-penetration of fluid, is calculated using the conservation laws. The Lagrangian force **F** is then distributed to the Eulerian mesh through a distribution function *D* (Eqs. 16, 17 and 18).

Using the momentum equations for compressible flows in the x and y directions, respectively, the components $F_x(\mathbf{x}_k, t)$ and $F_y(\mathbf{x}_k, t)$ can be calculated at a Lagrangian point $\mathbf{x}_k$ as:

$$F_x(\mathbf{x}_k, t) = \frac{\partial \rho u}{\partial t} - \left(-\frac{\partial \rho u^2}{\partial x} - \frac{\partial \rho uv}{\partial y} - \frac{\partial p}{\partial x} + \frac{\partial \tau_{xx}}{\partial x} + \frac{\partial \tau_{xy}}{\partial y} \right) \tag{10}$$

$$F_y(\mathbf{x}_k, t) = \frac{\partial \rho v}{\partial t} - \left(-\frac{\partial \rho uv}{\partial x} - \frac{\partial \rho v^2}{\partial y} - \frac{\partial p}{\partial y} + \frac{\partial \tau_{yx}}{\partial x} + \frac{\partial \tau_{yy}}{\partial y} \right) \tag{11}$$

All terms of equations (10) and (11) are determined by the interpolation of variables from the Eulerian grid, in a $\mathbf{x}_k$ position, at each instant of time t.

NUMERICAL METHOD

The terms of pressure gradient and inertia of the NSE are spatially discretized by using central finite volume scheme with second order accuracy named KT method [5]. An interpolation scheme using the minmod flux limiter [5,6] is applied to prevent the oscillations that occur when second order schemes are used for the NSE discretization in regions with shock, discontinuities or severe gradients. Viscous terms are discretized using central finite differences. The time integration was made explicitly by using first order Euler's method. The time step (Δt) is limited by the Courant number (CFL), using the following condition:

$$CFL = max\left(\frac{|u| + c}{\Delta x} + \frac{|v| + c}{\Delta y} \right) \tag{12}$$

where c is the local speed of sound.

Lagrangian and Eulerian forces calculation - CVPM

Equations (10) and (11) are solved on the Lagrangian points using interpolation schemes. For example, the terms $\frac{\partial \rho u}{\partial t}$ and $\frac{\partial \rho v}{\partial t}$ are responsible to enforce the fluid velocity as close as possible to the velocity of the immersed boundary. For this, these terms are calculated as:

$$\frac{\partial \rho u}{\partial t}(\mathbf{x}_k, t) = \frac{\rho(\mathbf{x}_k, t)\, u_{IB}(\mathbf{x}_k, t) - \rho(\mathbf{x}_k, t)\, u(\mathbf{x}_k, t)}{\Delta t} \tag{13}$$

$$\frac{\partial \rho v}{\partial t}(\mathbf{x}_k, t) = \frac{\rho(\mathbf{x}_k, t)\, v_{IB}(\mathbf{x}_k, t) - \rho(\mathbf{x}_k, t)\, v(\mathbf{x}_k, t)}{\Delta t} \tag{14}$$

where $u_{IB}(\mathbf{x}_k, t)$ and $v_{IB}(\mathbf{x}_k, t)$ are the Lagrangian velocities in x and y directions, respectively. $\rho(\mathbf{x}_k, t)$, $u(\mathbf{x}_k, t)$ and $v(\mathbf{x}_k, t)$ are calculated using the interpolated values from the Eulerian Cartesian grid. In the case of stationary body, the Lagrangian velocity of the boundary is zero.

In equations (10) and (11), the terms in brackets are the same

that appear on the right of equality in the momentum conservation equations in directions x and y, respectively. So, these terms can be calculated by interpolation from the spatial discretization of the momentum equation. After $F_x(\mathbf{x}_k,t)$ and $F_y(\mathbf{x}_k,t)$ being calculated in all Lagrangian points, these forces are distributed to the Eulerian mesh, producing a force field ($\mathbf{f}$) which is the source term of the NSE.

The interpolations from the Eulerian mesh are made using a distribution/interpolation function proposed by Peskin [1] and modified by Unverdi and Tryggvason [7]. For example, the value of the density in $\mathbf{x}_k$ can be interpolated from the Eulerian mesh using the following equation:

$$\rho(\mathbf{x}_k,t) = \sum_{i=1,j=1}^{N_x,N_y} D(\mathbf{x}_{i,j}-\mathbf{x}_k)\,\rho(\mathbf{x}_{i,j},t)\,\Delta x\Delta y \qquad (15)$$

$D(\mathbf{x}-\mathbf{x}_k)$ is the distribution function, which is calculated as the following equation:

$$D(\mathbf{x}-\mathbf{x}_k) = \frac{g(r_x)\,g(r_y)}{h^2} \qquad (16)$$

$$g(r) = \begin{cases} g_1(r) & if \quad \|r\| < 1 \\ \frac{1}{2} - g_1(2-\|r\|) & if \ 1 < \|r\| < 2 \\ 0 & if \quad \|r\| > 2 \end{cases} \qquad (17)$$

where:

$$g_1(r) = \left(3 - 2\|r\| + \sqrt{1+4\|r\|-4\|r\|^2}\right)/8 \qquad (18)$$

r_x and r_y are $(x_i-x_k)/h$ and $(y_i-y_k)/h$, respectively. h is the Eulerian grid size.

After the calculation of the force field in each Lagrangian point, the force is distributed to the Eulerian mesh, using the same distribution function $D(\mathbf{x}-\mathbf{x}_k)$ presented above. The Eulerian force field ($\mathbf{f}$) is obtained according to the following equation:

$$\mathbf{f}(\mathbf{x},t) = \sum_{k=1}^{N_p} D(\mathbf{x}-\mathbf{x}_k)\,\mathbf{F}(\mathbf{x}_k,t)\,\Delta s\Delta s \qquad (19)$$

where Δs is the distance between two Lagrangian points. The force field is effective only up to distance $2h$ and it has maximum intensity on the interface, according to the distribution function adopted.

An indicator function, $I(\mathbf{x},t)$ [7] allows the visualization/localization of the body. This function has value 0 outside the interface, value 1 inside the body and intermediary values on the interface. Since the present study aims to simulate adiabatic boundary, thermal conductivity was neglected inside the body using the indicator function to locate the cylinder. In the future an improvement for this process will be performed.

The drag and lift forces are obtained directly from the Lagrangian force through the integration on the interface.

RESULTS

The CVPM code was applied to study four problems involving two-dimensional flows over an isolated cylinder. In all these cases, the following gas properties are considered: molecular weight $MM = 28.96\ g/mol$, heat capacity ratio $\gamma = 1.4$ and Prandtl number $Pr = 0.71$. The initial conditions are pressure $p = 10^5\ Pa$ and density $\rho = 1.4\ kg/m^3$. The velocity of the undisturbed flow (u_∞) is calculated from the Mach number at the infinite (Ma_∞). In all studies a $1m$ diameter cylinder was considered. Reynolds number is calculated using the cylinder diameter. The viscosity of the gas is determined in each case to obtain the desired Re_∞.

Some of the simulations carried out with the CVPM code were also simulated using OpenFOAM. In OF the application rhoCentralFoam was used. It is a density based solver which uses the same discretization method [5] used in present work. The time integration is done implicitly through the first order Euler method. In the simulations with OF, an adaptive mesh was used and the VanLeer flux limiter [6] was applied.

The CFL number for all the simulations using the CVPM code is equal to 0.02, whereas the CFL number for all the simulations using OF is equal to 0.2. This low CFL requirement is due to the CVPM method.

Subsonic flow over an isolated cylinder

The results of subsonic flow over an isolated cylinder were obtained with both codes, CVPM and OF. For all these simulations, $Ma_\infty = 0.3$ and Re_∞ is equal to: 40, 80, 150 and 300. The domain is rectangular and its dimensions are $60D$ and $50D$ in the x and y directions, respectively. The cylinder center is located at $x = 22D$ and $y = 25D$.

Depending on the direction of the velocity vector in each cell, the boundaries are treated as inlets or outlets. At the inlets, the Dirichlet boundary conditions are applied for temperature and velocities and the Neumann boundary condition for pressure. At the outlets, the Dirichlet boundary conditions are applied for pressure and the Neumann boundary condition for temperature and velocities. The instantaneous results are shown as a function of non-dimensional time $\psi = tU_\infty/D$.

Two different grid refinements were used with the CVPM code. The maximum level of refinement of the meshes were equal to $\Delta x_{min} = D/80$ and $\Delta x_{min} = D/40$, with a total number of cells of 141,360 and 79,488, respectively. In figure 1 the coarse mesh with 79,488 cells is shown.

The OpenFOAM simulations were done using an adaptive mesh. The local maximum refinement is equal to $D/80$ over the cylinder and the total number of cells is 132,516. This mesh was built using the snappyHexMesh tool.

Symmetrical bubbles occurred on the flows at $Re_\infty = 40$. Figure 2 shows some geometrical parameters of the bubbles formed behind the cylinder. In Table 1, the results are shown for the simulations at $Re_\infty = 40$ together with some data from literature [4,8,9]. The computed geometrical properties of the symmetrical vortices agree quite satisfactorily with the literature specially the value b/D and the angle θ.

Table 2 summarizes some results obtained for simulations with Re_∞ equals 80, 150 and 300 using the CVPM code, OpenFOAM and from literature. The lift and drag coefficients have

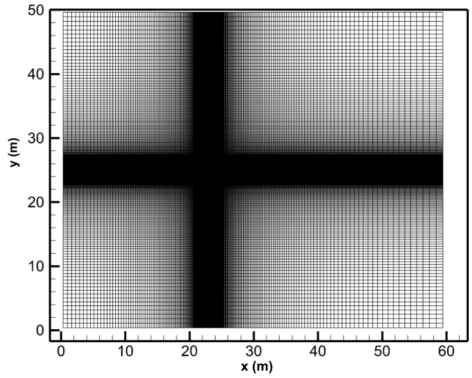

Figure 1. Coarse mesh with maximum refinement equal to $\Delta x_{min} = D/40$ and a total number of cells equal to 79,488.

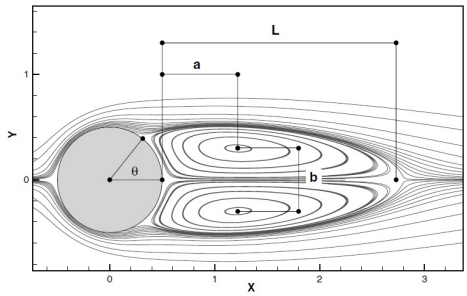

Figure 2. Relevant geometrical parameters of the symmetric separation region behind the cylinder. Source: [8].

Table 1. Bubble parameters and drag coefficient obtained with CVPM and OF codes, and simulations from literature at $Re_\infty = 40$.

	L/D	a/D	b/D	θ (°)	C_d
CVPM $\Delta x_{min} = D/40$	2.62	0.97	0.84	51.4	1.63
CVPM $\Delta x_{min} = D/80$	2.47	0.77	0.62	52.6	1.62
OF $\Delta x_{min} = D/80$	2.34	0.75	0.61	52.6	1.58
[4] (Numerical)	2.54	-	-	-	1.49
[8] (Numerical)	2.28	0.72	0.60	53.8	1.55
[9] (Experimental)	-	-	-	-	1.58

been time averaged over a number of shedding cycles. The computed Strouhal number based on the shedding frequency, f ($St = fD/U_\infty$) is also presented. The numerical results agree well with the experimental and numerical data from the literature. For $Re_\infty = 300$, the results are found to be in reasonable agreement due to the three-dimensional effects presented. When the refinement level is increased the results obtained with CVPM are closer to the results obtained with OpenFOAM.

Higher drag coefficients in the solutions obtained with the CVPM may be seen. This may be explained by considering that a compressible code was used to simulate the incompressible case ($Ma_\infty \leq 0.3$). The influence of the Mach number on the drag coefficient for these flows should be better investigated. All the presented reference data were obtained with incompressible codes and the results obtained with the OF also have higher drag coefficient when compared with literature.

In figure 3, the non-dimensional temperature (T/T_∞) field obtained for $Re_\infty = 150$ is shown. The maximum value is approximately 1.025, showing that at $Ma = 0.3$, the flow displays slightly compressible regime.

Table 2. C_d, C_l and St for Re_∞ equals 80, 150 and 300 flows.

Re_∞		C_d	C_l	St
80	CVPM $\Delta x_{min} = D/40$	1.49	±0.27	0.15
	CVPM $\Delta x_{min} = D/80$	1.45	±0.26	0.15
	OF $\Delta x_{min} = D/80$	1.42	±0.24	0.15
	[4] (Numerical)	1.40	±0.25	0.15
	[10] (Experimental)	-	-	0.15
150	CVPM $\Delta x_{min} = D/40$	1.44	±0.56	0.18
	CVPM $\Delta x_{min} = D/80$	1.43	±0.53	0.18
	OF $\Delta x_{min} = D/80$	1.40	±0.55	0.18
	[4] (Numerical)	1.37	±0.41	0.18
	[10] (Experimental)	-	-	0.18
300	CVPM $\Delta x_{min} = D/40$	1.57	±0.89	0.20
	CVPM $\Delta x_{min} = D/80$	1.53	±0.98	0.21
	OF $\Delta x_{min} = D/80$	1.45	±0.89	0.21
	[10] (Experimental)	-	-	0.22

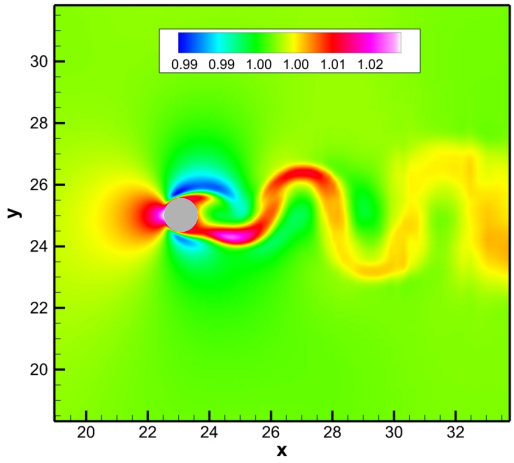

Figure 3. Non-dimensional temperature field obtained with CVPM for $Re_\infty = 150$ using the finest mesh with $\Delta x_{min} = D/80$.

Flow over a rotating cylinder

The flow over an isolated rotating cylinder at $Re_\infty = 200$ and $Ma_\infty = 0.3$ was simulated using CVPM and OF codes. In this study, the same mesh refinement and the same initial conditions

of the previous case were used. The angular velocity of the cylinder is 0.3 rad/s, so its peripheral velocity is equal to $u_\infty/2$.

In figure 4, the streamlines are shown for two different instant of time. The experimental results from literature [11] are also presented. The position and size of the recirculations are very well compared.

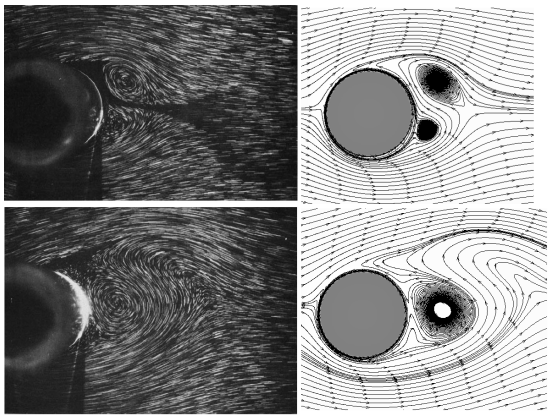

Figure 4. Streamlines obtained with CVPM (right side) for the rotating cylinder at $\psi = 1.5$ (top) and $\psi = 3.5$ (bottom). Left side experimental results [11].

In table 3, some parameters obtained for the rotating cylinder case are shown together with the reference data. Strouhal number compared well with both reference values. The drag is almost 4 % higher than the incompressible case [12]. The lift coefficient is very close to the result using OF code, but it was 7% lower than the incompressible simulation. In addition, it is known that compressible solvers when running under incompressible flow conditions (i.e. using low Mach numbers without corrections or preconditioning) do not provide the same aerodynamic quantities when compared to incompressible solvers. These results provide some guidelines and error estimates that quantify these differences and may need to be considered when running compressible solvers at incompressible flow regimes [13].

Table 3. Parameters obtained for the simulations of subsonic flow over an isolated rotating cylinder.

	C_d	C_l	St
CVPM $\Delta x_{min} = D/80$	1.40	1.09	0.19
OF $\Delta x_{min} = D/80$	1.37	1.11	0.19
[12] (Numerical)	1.35	1.17	0.19

Supersonic flow over an isolated cylinder

Flows at $Ma_\infty = 3$ and $Re_\infty = 500$ were modeled using CVPM and OF. The maximum level of refinement of the meshes is $\Delta x_{min} = D/100$, and the total number of cells is 146,880 and 141,126 for CVPM and OpenFOAM respectively. Is is a retangular domain having $30D$ and $40D$ in the x and y directions, respectively. The center of the cylinder is located at $x = 1.6D$ and $y = 20D$. For supersonic flows, the Dirichlet boundary conditions were applied for all variables on the left boundary, which is a supersonic inlet. For all the other boundaries, the Neumann boundary conditions were used.

The results are shown in non-dimension time equal to $\psi = 15$, when the steady state is achieved. The drag coefficients obtained with CPVM and with OF codes are 1.43 and 1.45, respectively. Figure 5, shows the pressure distribution obtained from a horizontal line passing through the cylinder center. The proximity between the pressure curves may be observed. There is a high gradient of pressure across the interface. Due to this gradient, it is difficult to determine the properties of the fluid at the interface. Temperature and density gradients also have the similar behavior.

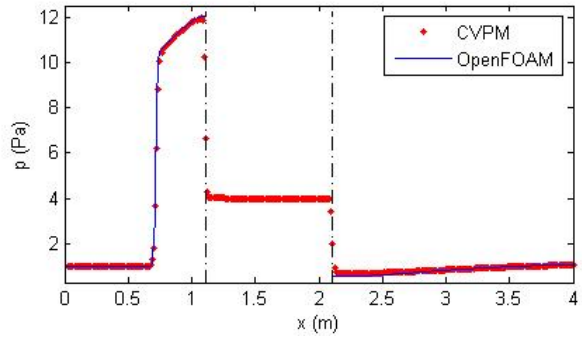

Figure 5. Pressure curves obtained for the flow at $Ma_\infty = 3$ and $Re_\infty = 500$. The dashed lines represent the position of immersed boundary.

Figure 6 presents Mach contours obtained with CVPM code. The symmetry of the flow can be seen. The solution also presents a fewer degree ripples in the shock region.

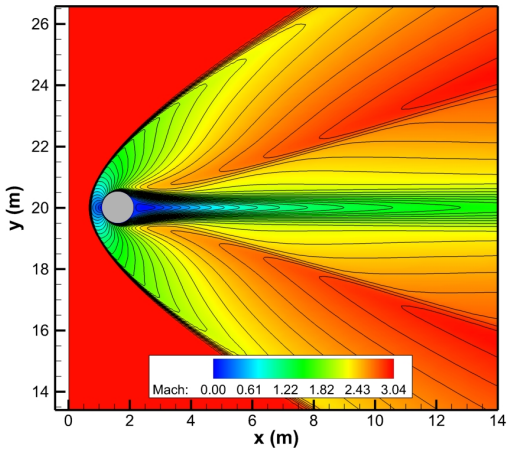

Figure 6. Mach number contours obtained with CVPM code. $Ma_\infty = 3$ and $Re_\infty = 500$.

Shock wave diffraction over an isolated cylinder

In this problem, the diffraction of a plane shock wave at $Ma = 2.81$ over an isolated cylinder was studied. The square domain has dimension of $8D$. The center of the cylinder is located at $x = 2.25D$ and $y = 4D$. The plane shock wave propagates in the

positive x direction, and at the beginning it is at $x = 0$. Reynolds number is equal to 10^3, and its calculation is done by taking the properties of the fluid in the shock wave region and the cylinder diameter.

A uniform Cartesian grid with 360,000 cells was used for modeling of this problem. The boundary conditions were the same as in the previous case. In the left boundary shock wave properties were imposed.

Non-dimensional density contours (ρ/ρ_∞) obtained by using the CVPM code at time $t = 3 \cdot 10^{-3}$ s are shown in figure 7. Experimental result from literature [14] is also presented.

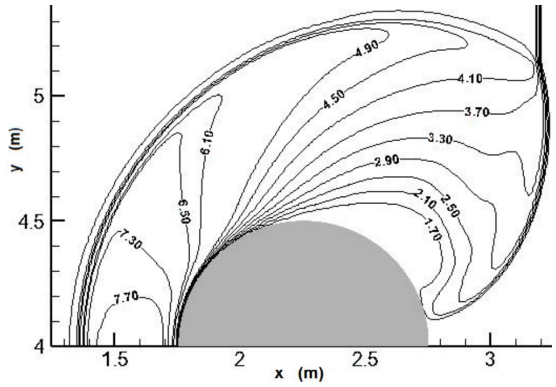

Figure 7. Non-dimensional density contours obtained by using the CVPM code at time $t = 3 \cdot 10^{-3}$ s.

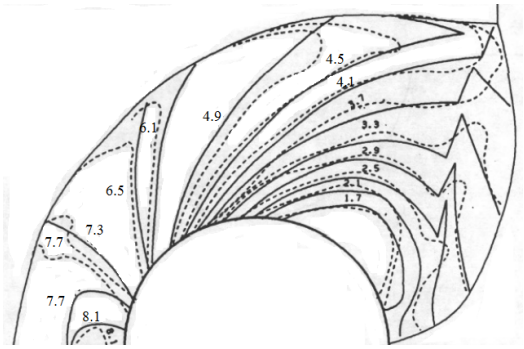

Figure 8. Non-dimensional density contours. Solid lines: experimental; dashed lines: Numerical. Source: [14].

The density field obtained by using CVPM code was very close to the experimental one [11]. This shows the capability of the method to simulate shock wave diffraction problems.

CONCLUSIONS

In this work, compressible laminar flows over a isolated cylinder were simulated using CVPM. Flows at Mach number ranging between 0.3 and 3 were studied. Good results were obtained, showing the CVPM ability to model flows in subsonic and supersonic regime. Parameters as the drag coefficient, lift coefficient and the Strouhal number were assessed and validated with literature data. The CFL number in the simulations had to be limited to 0.02 to use CVPM code. It is concluded that the CVPM is a simple implementation code which produced satisfactory results for compressible laminar flows over stationary and moving boundaries, however the computational cost is high due to limitation in the CFL number.

ACKNOWLEDGMENT

The authors would like to thank CNPq, FAPEMIG (Process APQ-02850-14 and APQ-0334-14) and CAPES (master scholarship) for their financial support.

REFERENCES

[1] Peskin, C. S., Flow patterns around heart valves: a numerical method, *Journal of computational physics*, v. 10, n. 2, 1972, pp. 252-271

[2] D. K. Clarke, H. A. Hassan, and M. D. Salas, Euler calculations for multielement airfoils using Cartesian grids. *AIAA Journal*, v. 24, n. 3, 1986, pp. 353-358

[3] Fadlun, E. A. and Verzicco, R. and Orlandi, P. and Mohd-Yusof, J., Combined immersed-boundary finite-difference methods for three-dimensional complex flow simulations. *Journal of Computational Physics*, v. 161, n.1, 2000, pp. 35-60

[4] Lima e Silva A. L. F., Silveira Neto A. and Damasceno J. J. R., Numerical simulation of two-dimensional flows over a circular cylinder using the immersed boundary method, *Journal of Computational Physics*, v.189, n.2, 2003, pp. 351-370

[5] Kurganov A. and Tadmor E., New high-resolution central schemes for nonlinear conservation laws and convection–diffusion equations, *Journal of Computational Physics*, v. 160, n. 1, 2000, p. 241-282

[6] Van Leer B., Towards the Ultimate Conservative Difference Scheme, V. A Second Order Sequel to Godunov's Method, *Journal of Computational Physics*, v. 32, 1979, pp. 101-136

[7] Unverdi S. O., and Tryggvason G., A front-tracking method for viscous, incompressible, multi-fluid flows, *Journal of computational physics*, v. 100, n. 1, 1992, pp. 25-37

[8] De Palma P., De Tullio M. D., Pascazio G., and Napolitano M., An immersed-boundary method for compressible viscous flows, *Computers & fluids*, v. 35, n. 7, 2006, pp. 693-702

[9] Triton D.J., Experiments on the flow past a circular cylinder at low Reynolds number, *Journal of computational physics*, v. 6, n. 4, 1959, pp. 547-567

[10] Williamson C. H. K., Defining a universal and continuous Strouhal-Reynolds number relationship for the laminar vortex shedding of a circular cylinder, *Phys. Fluids*, v. 31, n. 10, 1988, pp. 2742

[11] Coutanceau M. and Ménard C., Influence of rotation on the near-wake development behind an impulsively started circular cylinder, *Journal of Fluid Mechanics*, v. 158, 1985, pp. 399-446

[12] Silva A. R, Silveira Neto, A., Lima A. M. G. and Rade D. A., Numerical simulations of flows over a rotating circular cylinder using the immersed boundary method, *J. Braz. Soc. Mech. Sci. & Eng.*, v. 33, n. 1, 2011

[13] Kompenhans M., Ferrer, E., Rubio G. and Valero E., Comparisons of compressible and incompressible solvers: flat plate boundary layer and NACA airfoils, *2nd International Workshop on High-Order CFD Methods*, 2013

[14] Kaca J., An interferometric investigation of the diffraction of a planar shock wave over a semicircular cylinder, *NASA STI/Recon Technical Report N*, v. 89, 1988, pp. 16126